Lawrence Berkeley National Laboratory

LBL Publications

Title

High-Field Magnets for Future Hadron Colliders

Permalink

https://escholarship.org/uc/item/35m6p96d

Journal

Annual Review of Nuclear and Particle Science, 74(1)

ISSN

0163-8998

Author

Sabbi, GianLuca

Publication Date

2024-09-26

DOI

10.1146/annurev-nucl-102122-022007

Copyright Information

Peer reviewed

ANNUAL REVIEWS

Annual Review of Nuclear and Particle Science

High-Field Magnets for Future Hadron Colliders

GianLuca Sabbi

Accelerator Technology and Applied Physics Division, Lawrence Berkeley National Laboratory, Berkeley, California, USA; email: glsabbi@lbl.gov

ANNUAL REVIEWS CONNECT

www.annualreviews.org

- Download figures
- Navigate cited references
- Keyword search
- Explore related articles
- Share via email or social media

Keywords

high-energy colliders, superconducting accelerator magnets, niobium–tin, high-temperature superconductors

Abstract

Recent strategy updates by the international particle physics community have confirmed strong interest in a next-generation energy frontier collider after completion of the High-Luminosity LHC program and construction of a e^+e^- Higgs factory. Both hadron and muon colliders provide a path toward the highest energies, and both require significant and sustained development to achieve technical readiness and optimize the design. For hadron colliders, the energy reach is determined by machine circumference and the strength of the guiding magnetic field. To achieve a collision energy of 100 TeV while limiting the circumference to 100 km, a dipole field of 16 T is required and is within the reach of niobium–tin magnets operating at 1.9 K. Magnets based on high-temperature superconductors may enable a range of alternatives, including a more compact footprint, a reduction of the cooling power, or a further increase of the collision energy to 150 TeV. The feasibility and cost of the magnet system will determine the possible options and optimal configurations. In this article, I review the historical milestones and recent progress in superconducting materials, design concepts, magnet fabrication, and test results and emphasize current developments that have the potential to address the most significant challenges and shape future directions.

Contents

1. INTRODUCTION

High-field superconducting magnets control the beam trajectories in hadron colliders and ultimately determine the machine performance and discovery potential. The Tevatron magnet system, which is based on the ductile niobium–titanium (Nb-Ti) alloy, was the first large-scale application of superconductivity and a major breakthrough in both energy reach and power consumption (1). Further development by the HERA, UNK, SSC, RHIC, and LHC projects led Nb-Ti technology to full maturity (2). The LHC design field of 8.3 T is regarded as a practical limit for Nb-Ti dipoles in a large accelerator (3).

After intensive and prolonged R&D efforts, niobium–tin (Nb_3Sn) has emerged as the first fully engineered material that can expand the field reach of accelerator magnets beyond 10 T (4). Nb_3Sn technology is on the verge of delivering a major contribution to particle physics by enabling a 10-fold increase of the integrated luminosity of the LHC (5). This achievement is only a first step toward future energy frontier colliders. Significant performance optimization and process scale-up efforts are needed to prepare for large-scale production of Nb_3Sn dipoles in the range of 12 to 16 T (6). High-temperature superconductors (HTS) may enable further progress to 20 T and beyond, but achieving these performance levels requires addressing more fundamental challenges. This article presents a summary of the most significant past results and next steps to meet the requirements of future hadron colliders at the energy frontier.

2. ACCELERATOR REQUIREMENTS

High-energy colliders place unique requirements on the magnet system. Very large machine circumference and cost require a complex optimization effort. The coil layout must be compact and

efficient to minimize conductor volume, electromagnetic stored energy, forces, and associated mechanical support components. This implies selecting the smallest aperture compatible with beam stability and the cryogenic vacuum system design. Likewise, compact coil ends and short interconnections are needed to achieve high longitudinal fill factors. A dynamic range above 15 is desired to minimize the cost of the injectors. This requires efficient ramping of many magnets in series between injection and collision to maximize the time spent in luminosity production. Stringent field quality specifications must be met across the operational range to preserve the beam characteristics and avoid losses. Finally, to maximize the physics reach, the magnets should be operating as close as possible to the critical surface, which determines the boundary of the superconducting phase as a function of temperature, field, and current density.

To balance these demands, it is necessary to develop the magnet system in the context of an integrated design effort for a next-generation collider. At present, the Future Circular Collider (FCC)[1] (7) and the Super Proton–Proton Collider (SPPC)[2] (8) projects provide the most relevant frameworks for magnet development. Both designs initially adopted a 100-km reference circumference with either 16-T (FCC) or 12-T (SPPC) dipoles. The 16-T dipole may also enable a 26-TeV High-Energy LHC (HE-LHC)[3] in the existing tunnel (9). **Table 1** shows the initial machine parameters for the proposed colliders compared with LHC parameters. Alternative configurations and upgrades are being actively investigated. In particular, after completion of the FCC Conceptual Design Report (CDR), a feasibility study is underway to optimize the machine configuration and implementation plan. Taking into account geology, surface constraints, and available infrastructure, a ring placement with a circumference of 90.7 km was selected (10). This layout provides a basis for technical and cost studies investigating a dipole field range of 14 to 20 T in coordination with the magnet R&D effort. For SPPC, the plan includes a longer-term

Table 1   HE-LHC, FCC, and SPPC parameters compared with LHC parameters

Parameter (unit)	LHC[a]	HE-LHC[b]	FCC[c]	SPPC[d]
Collision energy (TeV)	14	25.8	100	75
Circumference (km)	26.7	26.7	97.75	100
Dipole field (T)	8.3	16	16	12
Operating temperature (K)	1.9	1.9	1.9	4.2
Arc filling factor	0.79	0.77	0.80	0.78
Dipole magnetic length (m)	14.3	13.7	14.1	15.0
Number of dipoles	1,232	1,232	4,668	4,360
Aperture (mm)	56	50	50	50
Aperture separation (mm)	194	250	250	300

Abbreviations: FCC, Future Circular Collider; HE-LHC, High-Energy LHC; SPPC, Super Proton–Proton Collider.
[a]Parameters from LHC Design Report (11).
[b]Based on Conceptual Design Report configuration with 23 cells per arc and LHC-like optics (9).
[c]Conceptual Design Report parameters from Reference 7.
[d]Reference parameters from Reference 8.

[1]The FCC study examines electron–positron, proton–proton, and heavy-ion collisions. Here we refer to the hadron collider (FCC-hh).
[2]The SPPC is conceived as a stage 2 project following a Circular Electron–Positron Collider (CEPC) in the same tunnel.
[3]A previous HE-LHC study aimed at an energy of 33 TeV combining high-temperature superconductors (HTS) and low-temperature superconductors (LTS) to achieve a 20-T dipole field (12).

upgrade with dipole fields up to 24 T. In the following sections, we review the most critical collider requirements from a magnet design perspective.

2.1. Operating Field and Temperature

The FCC CDR operating field of 16 T with a 14% margin on the load line translates to a conductor-limited (short sample) dipole field of 18.6 T. The baseline dipole design (6) achieves this performance using a magnetically optimized twin-aperture cross section with a total conductor area of 131 cm^2 (7). The required critical current density of 1.2 kA mm^{-2} at the coil peak field of 19 T and operating temperature of 1.9 K correspond to the FCC Nb$_3$Sn conductor development target (18) using established scaling relations. These parameters can be considered as a practical limit due to the steep reduction of the critical current density with increasing field (**Figure 1**). In fact, the 16-T dipole cross section almost doubles the conductor area relative to the LHC Nb-Ti arc dipole. Further increasing the short sample field by just 4% would result in a 30% larger coil (19).

In the case of SPPC, a 12-T operating field was selected for the baseline machine (14- to 15-T short sample, depending on the required margin). This choice results in a 25% reduction of the collision energy for the same machine circumference as FCC but allows for consideration of several cost-saving alternatives, such as a reduced conductor area or simpler coil configurations that may be magnetically less efficient but easier to fabricate at large scale. Lower electromagnetic

Figure 1

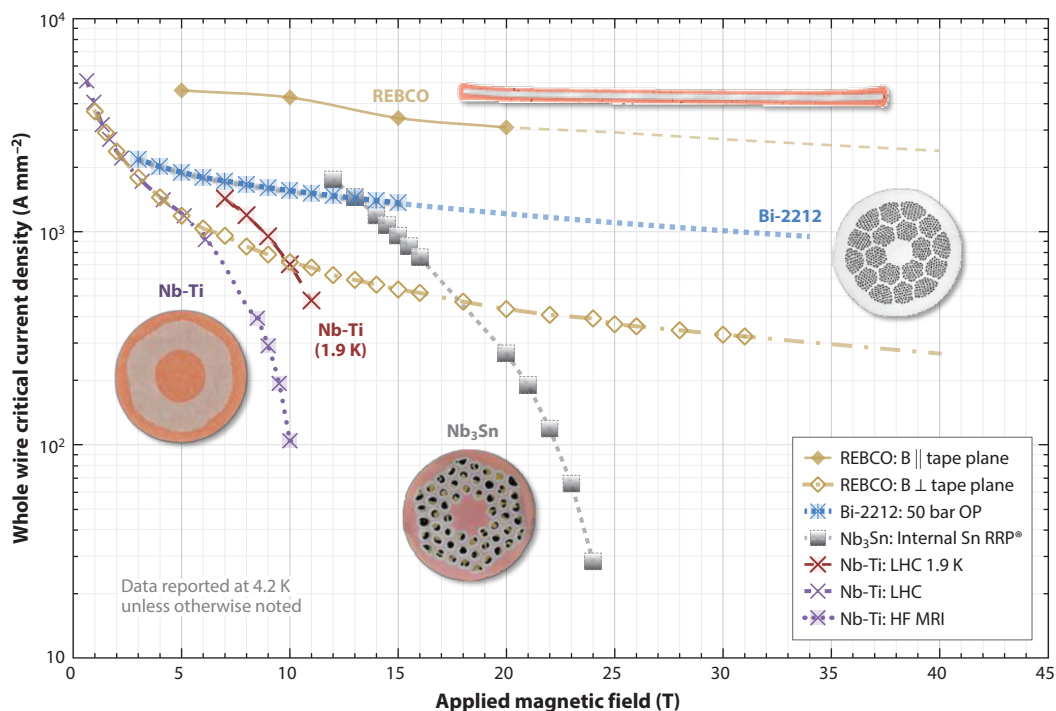Selected high-performance wires and tapes that are commercially available in long and uniform piece lengths: Nb-Ti (13, 14), Nb$_3$Sn (15), Bi-2212 (16), and REBCO (17). Abbreviations: HF MRI, high-field magnetic resonance imaging; OP, overpressure; RRP, Restacked Rod Process. Figure adapted with permission from Peter Lee (NHMFL/FSU) (**https://fs.magnet.fsu.edu/~lee/plot/plot.htm**; CC BY 4.0).

forces and stored energy simplify the requirements for mechanical support and quench protection. Replacing Nb_3Sn with future iron-based superconductors may reduce the cooling power needs.

A dipole field range of 20 to 24 T is compatible with the fundamental properties of the best-performing HTS. However, realizing this potential will require significant technology break-throughs and possibly new approaches to the beam physics and accelerator design. The special characteristics of the interaction region (IR) quadrupoles could make them suitable candidates for a first, smaller-scale deployment of HTS technology in the collider, as for Nb_3Sn in the High-Luminosity LHC (HL-LHC). The selection of the dipole operating field and temperature will ultimately depend on the performance and cost of the magnet technology options that will be available at the time of construction.

2.2. Collider Layout and Beam Vacuum System

The horizontal twin-aperture layout (**Figure 2*a***) was adopted as the baseline for the FCC CDR. It is efficient both magnetically, using the flux return of each aperture to enhance the field in the other, and mechanically, compensating for the horizontal forces acting between the two apertures. A vertical arrangement with larger winding radii has potential advantages for conductor compatibility and is the primary focus of the SPPC magnet program (**Figure 2*b***).

Each FCC 50-TeV beam, traveling in a 16-T dipole field, emits a synchrotron radiation power of 29 W m^{-1}. This value is almost two orders of magnitude higher than that achieved at the HL-LHC, making the beam vacuum system one of the most challenging elements of the collider. A novel beam screen was developed to accommodate the beam envelope, mitigate instabilities due to electron cloud and impedance effects, ensure high vacuum, and limit the heat load in the cryogenic system (20). The resulting minimum magnet aperture is 50 mm in FCC, and the same value was selected for SPPC. A similar aperture is foreseen to be adequate for a higher-energy collider based on 20- to 24-T magnets.

Particle collisions at the interaction points are the main sources of beam loss at hadron colliders. This effect leads to a useful beam lifetime of about 3.5 h in FCC-hh compared with about 8 h at the LHC (22). The time allocated for ramping the magnets from injection to collision field is 20 min, and another 20 min is allocated for the down-ramp, corresponding to approximately 37%
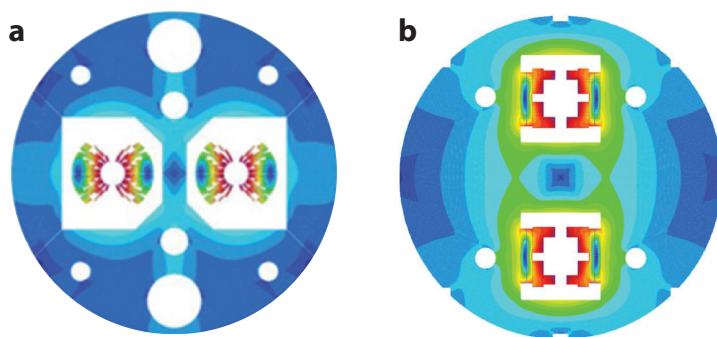
Figure 2

(*a*) Future Circular Collider (FCC) dipole design option with horizontal twin-aperture layout. (*b*) Super Proton–Proton Collider (SPPC) dipole design option with vertical twin-aperture layout. The magnetic field in the superconducting coil and iron yoke is shown by colored contour zones. In panel *a*, the maximum field (*red*) is 16.4 T at a 16-T central field. In panel *b*, the maximum field (*red*) is 16.0 T at a 15-T central field. For both cases, the minimum field (*dark blue*) is zero. Panel *a* adapted from Reference 7 (CC BY 4.0). Panel *b* adapted with permission from Reference 21 and Qingjin Xu (IHEP).

of the target turnaround time. From a magnet design standpoint, the key issues limiting the ramp rate are control of eddy current effects affecting the thermal margin and field quality during the ramp.

The highly optimized dipole fill factor of 0.78 achieved at the LHC provides a reference for future colliders. The length of individual magnets is limited to 14–15 m by the requirements for mass production, transport, qualification testing, and installation in the tunnel. Therefore, a critical design consideration is to minimize the longitudinal space allocated to magnet terminations and interconnections. Fill factor considerations are also prompting a reexamination of the combined function optics, where the dipole coils are designed to include a quadrupole component, effectively eliminating the quadrupole magnets from the lattice (23). Magnet analysis is required along with more detailed accelerator physics studies to explore the complex trade-offs of this solution relative to the standard separated-function lattice, which has been used in all superconducting accelerators to date.

2.3. Field Quality

Nonlinear field components can cause beam particles to drift away from the core and eventually get lost. Tracking studies determine the phase-space amplitude (dynamic aperture) required to ensure sufficient lifetime and the corresponding limits on the field errors.

In the magnet straight section, the field is fully contained in the transverse (x–y) plane and can be expressed in terms of harmonic coefficients defined by the power series expansion

$$B_y + iB_x = B_1 10^{-4} \sum_{n=1}^{\infty} (b_n + ia_n) \left(\frac{x + iy}{r_0} \right)^{n-1}, \qquad 1.$$

where B_x and B_y are the horizontal and vertical field components, and b_n and a_n are the normal and skew n-pole harmonic coefficients. The multipole coefficients are conveniently expressed in 10^{-4} units of the dipole field B_1 ($b_1 = 10^4$). The reference radius r_0 is chosen to correspond to the beam-populated region—approximately 50% of the aperture in modern colliders. The same expansion can be extended to the field integrals across the magnet end regions. Detailed orientation and powering conventions are required to properly interface magnetic measurements and beam studies (24).

The arc dipole field quality is particularly critical at injection because of the sextupole and decapole components generated by conductor magnetization (25). These effects are a primary factor driving the conductor and corrector magnet requirements.

After the beams are brought into collision, the dynamic aperture is dominated by the field quality of the IR quadrupoles, where the beam undergoes large amplitude oscillations while being focused toward the interaction points. The development of Nb_3Sn IR quadrupoles for the HL-LHC provides detailed information about errors generated by geometric tolerances, persistent currents, and the effects of cooldown and magnetic forces (26). The resulting field quality has been shown to be adequate for the HL-LHC and is also expected to be adequate for future hadron colliders.

3. PROGRESS IN NIOBIUM–TIN ACCELERATOR MAGNETS

Nb_3Sn was discovered in 1954 (27), and it was soon recognized that its properties suggested "the feasibility of constructing superconducting solenoid magnets capable of field approaching 100 kgauss" (28, p. 89). Its upper critical field (B_{c2}) of 30 T and critical temperature (T_c) of 18.3 K approximately double the respective Nb-Ti values (29).

Dynamic aperture: amplitude of the position–momentum phase space where long-term stability of the particle motion is achieved

A key milestone was achieved in the mid-1970s with the development of high-current-density multifilament wires using the Internal-Tin process (30). However, Nb_3Sn is formed at high temperature, and the resulting compound is brittle and strain sensitive. These factors bring significant challenges in accelerator magnet applications compared with the ductile Nb-Ti alloy. About 20 years of pioneering studies in Europe, Japan, and the United States (31, 32) were required for Nb_3Sn dipoles to surpass the Nb-Ti field limits. In the mid-1990s, the University of Twente MSUT model reached 11 T at 4.2 K (33), and soon afterward, LBNL's D20 reached 13.5 T at 1.9 K (34). These magnets were based on a new wind-and-react process, in which cabling and coil winding are performed using precursor wires, and Nb_3Sn is formed in the final coil geometry by high-temperature heat treatment at 650–700°C. To withstand the high reaction temperatures, fiberglass insulation replaced polyimide, and metal components replaced composites used in Nb-Ti magnets. After reaction, vacuum pressure impregnation with epoxy resins was applied to protect the fragile conductor from stress concentration during magnet assembly and powering.

With further advances in high-performance wires (35) and mechanical assembly methods (36), by 2004 the LBNL RD (37) and HD (38) models had demonstrated consistent performance in the range of 14–16 T at 4.2 K. These results prompted the US Department of Energy (DOE) to launch the LHC Accelerator Research Program (LARP), a collaboration of BNL, Fermilab, and LBNL working with CERN to develop Nb_3Sn IR quadrupoles for the HL-LHC (39). Following a successful R&D phase (40), the program transitioned to prototyping and production both in the United States (41) and at CERN (42). In parallel, new research initiatives are getting underway worldwide to address the needs of post-LHC colliders (43). The main achievements and outstanding challenges of Nb_3Sn technology are reviewed in the following sections.

3.1. Wire and Cable

Conductors for high-field accelerator magnets are designed to satisfy a complex set of requirements. High current capacity is needed to limit the magnet inductance, enabling series powering of many units in the same circuit and a fast discharge in case of a magnet quench or other fault condition. However, flux-jump instabilities severely limit the current that can be carried by a single superconducting filament. High resistivity of the superconductor after transition to the normal state requires a low-resistance current bypass to limit Joule heating following a quench. Field quality considerations demand precise control of magnetization and eddy current effects over the entire operational range. These challenges are addressed using a two-stage conductor design. The first stage is a round wire composed of many thin superconducting filaments embedded in a pure copper matrix. At the second stage, a high-current cable is fabricated using several tens of twisted and fully transposed wires. The following subsections detail the physics and engineering considerations that drive the development and optimization of Nb_3Sn conductors for accelerator magnets. The most successful cabling approach, named after the Rutherford Appleton Laboratory where it was originally developed, is described in the sidebar titled Rutherford Cables.

3.1.1. Precursor wires. High-performance Nb_3Sn conductors originate from programs launched in the 1990s to establish a commercial supply of wires optimized for the high-energy physics (HEP) community. The US DOE Conductor Development Program (45) aimed for high critical current density (>3 kA mm^{-2} at 12 T and 4.2 K), small effective filament diameter (<40 μm), long piece length with uniform properties (>10 km), and affordable cost (<$1.5 per kiloampere-meter at 12 T and 4.2 K). The Next European Dipole (46) had similar goals with a focus on larger-diameter wires (1.25 mm versus 0.3–1.0 mm in the United States). Two leading candidates, both belonging to the Internal-Tin category, emerged from these efforts: the Restacked Rod Process (RRP), developed by Oxford Superconducting Technology (OST) in

Quench: progressive transition from superconducting to normal state; quench usually starts with a local disturbance and propagates to the surrounding areas due to resistive heat generation

Restacked Rod Process (RRP): precursor wire fabrication method based on Nb rods

RUTHERFORD CABLES

Rutherford-type cables (44) enable design currents of 5 to 20 kA in superconducting accelerator magnets, as required by series-powering and quench protection considerations. Two layers of twisted and fully transposed wires are arranged in a flat geometry (**Figure 3d**). The resulting rectangular or slightly trapezoidal cross section and bending capabilities are well suited to winding accelerator-type coils that are magnetically efficient and can withstand high mechanical loads. Interstrand resistances can be adjusted to control coupling losses while ensuring sufficient current sharing for stability and protection. These combined characteristics have made Rutherford-type cables an invaluable cornerstone of accelerator magnet technology.

the United States (15); and the Powder In Tube (PIT) process, developed by Shape Metal Innovations (SMI) in Europe (47). Both processes aim at the fabrication of precursor wires with geometry and composition that will yield high Nb_3Sn formation with the desired properties after coil reaction.

The RRP process starts with the fabrication of a subelement by extrusion of a stack of Nb rods encased in a copper matrix with a central Sn core and surrounded by an Nb-based Sn diffusion barrier. The subelement is then restacked to a hexagonal pattern, extruded, and drawn to the final wire diameter. During the conductor heat treatment, Sn diffuses through the copper matrix and combines with the Nb rods and the inner portion of the Nb barrier to form Nb_3Sn. The number of subelement sites scales with n, the number of layers in the hexagonal pattern, as $3n(n-1)+1$. The central layers are occupied by pure copper for stability and quench protection. Different architectures are characterized by the number of sites occupied by the Nb_3Sn precursor subelements and the total number of sites. For example, a 108/127 design has seven layers of subelements; the inner three are made of pure copper, and the outer four are made of Nb_3Sn. Typical cross sections for wires used in accelerator magnets are shown in **Figure 3a,b**.

RRP wires achieve high critical current density by increasing the Nb and Sn fractions within the subelement, with Nb_3Sn forming in 30% of the wire cross section, and by enabling homogeneous diffusion of Sn to the Nb rods during heat treatment (49). However, this process results in a connected ring of Nb_3Sn of the same size as the subelement (in the range of 35 to 100 μm). Therefore, the entire subelement behaves like a single superconducting filament, with negative implications on wire magnetization, stability, and strain sensitivity. Reducing the subelement size by increasing the number of layers has proved challenging (50). At present, designs with

Powder In Tube (PIT): precursor wire fabrication method based on Nb tubes

a   **b**   **c**   **d**   **e**
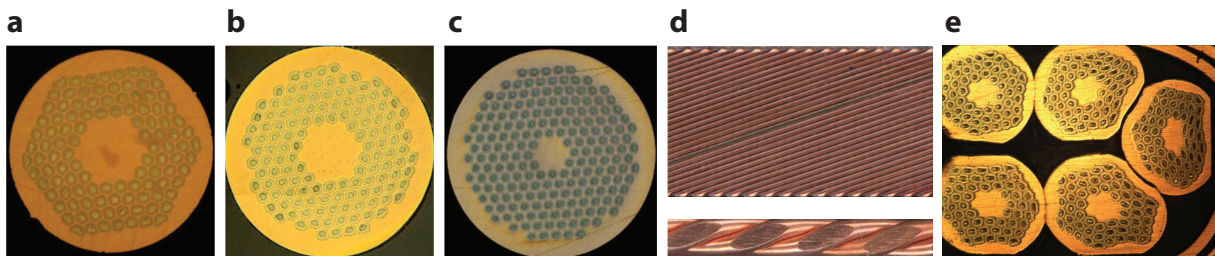
Figure 3

(*a–c*) RRP and PIT wires of 0.85-mm diameter used in the High-Luminosity LHC short model program: (*a*) RRP 108/127, (*b*) RRP 132/169, and (*c*) PIT 192. (*d*) Top and side views (not in scale) of the HD2 cable with 22-mm width and 1.4-mm thickness. (*e*) Detail of the wire deformation at the edge of the cable shown in panel *d*. Abbreviations: PIT, Powder In Tube; RRP, Restacked Rod Process. Panels *a–c* reproduced with permission from Reference 48. Panels *d* and *e* adapted from Reference 38 (CC BY 4.0).

127 subelements are suitable for wire diameters of 0.8 to 0.9 mm; such a design was adopted for the HL-LHC IR quadrupole production (51). A subelement count of 169 is preferred for larger wires in the diameter range of 1.0 to 1.1 mm, which are of primary interest for the innermost coil layers of future arc dipoles (7).

In the SMI-PIT process (**Figure 3c**), subelements are fabricated from Nb tubes filled with an Sn-based powder. This process demonstrated a 192-subelement layout with good properties but was considered less attractive than RRP in terms of overall performance and cost. For these reasons, it was not selected for HL-LHC IR quadrupole production despite having been used successfully in several short models (52).

3.1.2. Stability.

The combination of high critical current and large filament diameter makes advanced Nb_3Sn wires vulnerable to magneto-thermal instabilities, where the magnetic flux or electric currents suddenly redistribute within the subelements, generating sufficient heat to cause a quench—that is, a sudden transition to the normal state (53).

A filament diameter below 20 µm is required for adiabatic stability, but so far it has not been possible to achieve this target without negatively affecting the overall conductor performance. Therefore, advanced wires rely on dynamic stability by ensuring efficient transfer of the generated heat to the copper matrix. The low-temperature thermal conductivity of copper depends on its purity and can be characterized in terms of residual resistivity ratio (RRR). A copper RRR above 100 is generally sufficient to avoid premature quenches in magnet operation (54, 55). However, any Sn leakage through the diffusion barrier, due to overreaction, localized defects, or damage during cabling and coil fabrication, can degrade the copper RRR and potentially limit the magnet performance. These considerations contribute to the selection of the optimal reaction temperature and time, to balance J_c and RRR. Conductor damage due to excessive stress during magnet assembly and powering can also cause unstable behavior since the current density may increase above the stability threshold to bypass the damaged sections (56).

3.1.3. Strain sensitivity.

The critical current density of Nb_3Sn depends on the applied mechanical strain (59). In a limited range, the strain sensitivity is associated with a change of the upper critical field and is reversible (60). Outside this range, cracks start to form in the Nb_3Sn phase, leading to permanent degradation. Measurements of critical current as a function of axial strain are used to optimize the wire layout, composition, and heat treatment. It is particularly important not to exceed the intrinsic irreversible axial strain limit $\varepsilon_{irr,0}$, which denotes the start of permanent degradation. Studies performed in support of the HL-LHC IR quadrupole development (**Figure 4a**) resulted in a significant improvement of $\varepsilon_{irr,0}$ using Ti doping instead of Ta doping (61). Another key finding was that lower reaction temperatures of approximately 640°C, used to maintain high RRR, caused a severe reduction of $\varepsilon_{irr,0}$ (57). In response to these findings, the Nb/Sn ratio was increased from 3.4 to 3.6 to optimize critical current density and RRR at a higher reaction temperature of 665°C (50). The resulting $\varepsilon_{irr,0}$ is 0.25% in the HL-LHC wires.

Measurements performed under axial strain are not easily extrapolated to the magnet condition where wires are cabled, wound in coils, and impregnated with resin. Furthermore, the highest loads are usually applied in the transverse direction, and degradation limits should be determined both at room temperature (for magnet assembly) and at cold temperatures. Wire measurement techniques can be extended to include transverse mechanical stress as shown in **Figure 4b** (58). It is also possible to use computational approaches to correlate transverse and axial strain effects (62). Critical current measurements of impregnated cables under transverse stress are more directly applicable but are also more difficult to perform, and the background field is limited to 10–15 T (63, 64). Combining results from wire and cable studies, the transverse stress limits for permanent degradation in RRP wires can be set to 120 MPa at room temperature and 150–200 MPa after cooldown (42).

Residual resistivity ratio (RRR): ratio of the electrical resistivity at 273 K divided by its value at 20 K; RRR is related to thermal conductivity and is important for wire stability

Mechanical strain: ratio of the total deformation to the initial dimension of a material body in response to an external force or load (usually denoted by ε and expressed as a percentage)

Mechanical stress: force applied per unit area (denoted by σ); in elastic materials, stress is related to strain through the material's modulus of elasticity E: $\sigma = E\varepsilon$
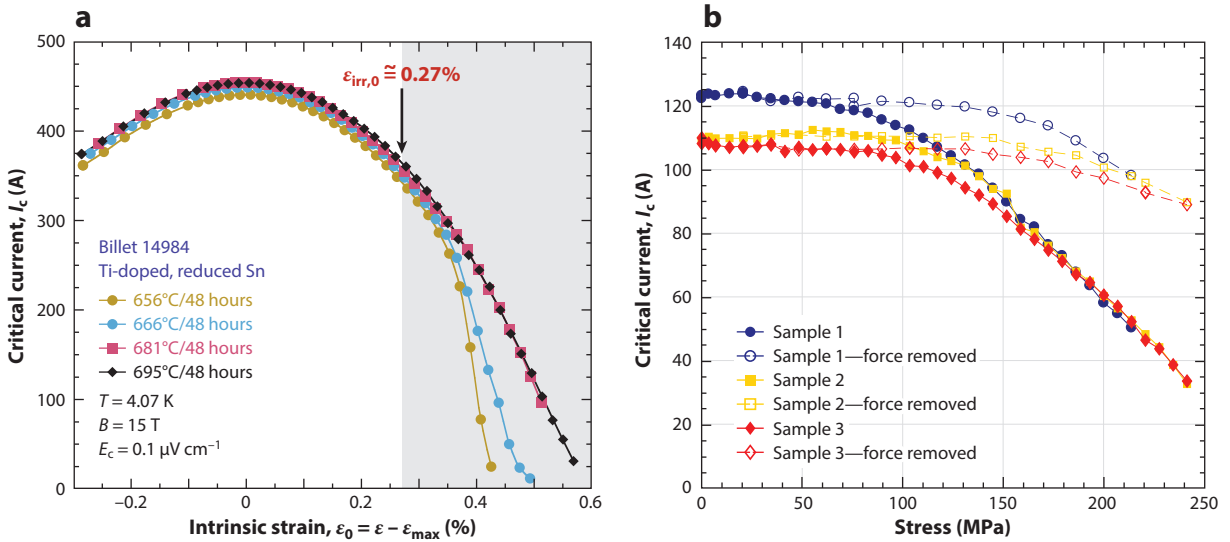
Figure 4

Critical current (I_c) dependence on mechanical loads in Restacked Rod Process 108/127 wires used in the High-Luminosity LHC interaction region quadrupoles. (*a*) Longitudinal strain at 15 T. (*b*) Transverse stress at 19 T. Panel *a* adapted from Reference 57 (CC BY 4.0) with permission from Najib Cheggour (NHMFL/FSU). Panel *b* adapted from Reference 58 (CC BY 4.0) with permission from Jose Ferradas Troitino (CERN) and Carmine Senatore (Univ. Geneva).

3.1.4. Radiation effects. Irradiation experiments of Nb_3Sn wires have been performed at research reactors and characterized as a function of integrated neutron fluence. Since impurities and dislocations can act as pinning centers, the critical current density initially increases with dose until more extensive damage occurs and J_c starts to degrade. Studies performed on MQXF wires showed that J_c is still improving at $1–2 \times 10^{18}$ cm^{-2} (65), which is sufficient to maintain the required conductor performance over the machine lifetime.

3.1.5. Rutherford cables. Rutherford cable optimization is more challenging for Nb_3Sn than for Nb-Ti. Preserving the integrity of the diffusion barrier is essential to avoid contamination of the high-purity stabilizer during reaction. Plastic deformation of the subelements can also result in critical current degradation and increased effective filament size (66).

Extensive cable optimization studies were performed during the LARP program (67). Most damage occurs at the cable extremities, where the edge compaction is concentrated due to friction effects. For this reason, the cable width is increased by a few percent from the theoretical width, defined as $W_{th} = dN/2\cos(\phi)$, where d is the strand diameter, N is the number of strands, and ϕ is the pitch angle. The cable thickness is less critical and may be slightly reduced to improve mechanical stability. Keystone angles are limited to about half the range of similar Nb-Ti cables. Starting from these general guidelines, each individual cable is optimized with feedback from winding tests, metallography, and electrical characterization of extracted strands to achieve adequate mechanical stability, RRR > 100, and critical current degradation below 3–5%.

Large eddy currents were observed in early Nb_3Sn cables with detrimental effects on cryogenic heat loads, temperature margin to quench, and field quality. Strand coatings used to control the interstrand resistance in Nb-Ti cables are not applicable due to the high-temperature heat treatment. The LARP program demonstrated that a thin stainless-steel core inserted between strand layers is effective in preventing sintering during reaction (68). A core width approximately 60% of
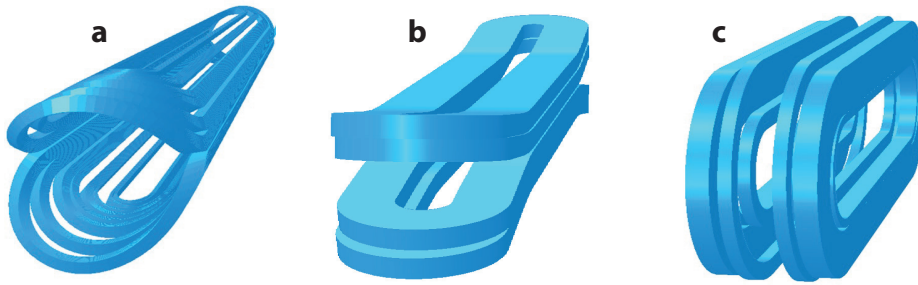
Figure 5

Examples of dipole coil windings: (*a*) cos θ coil with saddle ends, (*b*) block coil with flared ends, and (*c*) common coil with racetrack ends. Single-aperture windings are shown except for the common coil, which is intrinsically a twin-aperture configuration.

the cable width provides strong reduction of the eddy current effects (69) while preserving sufficient current sharing for stability (70). However, the core is incompatible with a two-step cabling process, starting with slightly larger geometry, followed by anneal and reroll to the target dimension. Using a single-step cabling process required modifications of the coil fabrication tooling and procedures to cope with reduced mechanical stability and larger-dimensional changes during reaction (71).

3.2. Coil Design and Fabrication

The most established coil layout for accelerator magnets (**Figures 2a** and **5a**) approximates a cos($n\theta$) current distribution[4] using keystone Rutherford cables and wedges (72). With a self-supporting Roman arch structure and efficient use of superconductor, it has been used in all past colliders and has been the main focus of Nb_3Sn magnet development (4). The LARP program performed a systematic coil design optimization that included component selection (73), tooling to accommodate volumetric changes during reaction (74), scale-up to a length of 3.3 m (75), and robust electrical insulation and process uniformity (71). However, the HL-LHC accelerator design called for a significantly larger aperture size and length compared with those in the LARP R&D models (76). A vigorous program at CERN and in the United States was implemented to address the new requirements, further strengthen the insulation system, and identify and correct nonconformities. Coil production for the 4.2-m-long US-built magnets is now well advanced (77). The 7.3-m-long CERN-built magnets have completed their prototyping phase (42).

Due to its magnetic efficiency and extensive past developments, the cos θ layout continues to be the primary reference for Nb_3Sn magnets. However, alternative approaches to coil design and fabrication are being actively explored. Among them is the block-coil layout, where a rectangular Rutherford cable is wound with its wide side parallel to the main dipole field (**Figure 5b**). This concept brings potential advantages for cable design and stress distribution but requires a structural bore supporting the coil and a flared geometry to clear the bore at the magnet ends (38). The common-coil configuration (**Figures 2b** and **5c**) takes advantage of a vertically arranged twin-aperture layout to replace the traditional coils with larger-radius windings shared between both apertures (78). Similar to block coils, a bore structure is required along with modifications of the flat racetrack geometry and/or auxiliary coils to achieve good magnetic efficiency and field quality (79, 80).

---

[4]Here, the variable *n* denotes the multipole order of the generated field: $n = 1$ for a dipole, $n = 2$ for a quadrupole, etc.

Accelerator coils traditionally have been optimized for magnetic efficiency, maximizing the current density in close proximity to the bore. However, future high-field magnets may require force bypasses to protect the conductor from excessive stress. This concept was first implemented in a block-coil split in sections by a system of piers and beams (81). More recent proposals use grooved mandrels where groups of cables (or, in a limiting case, individual turns) are inserted. This approach is applicable to the traditional coil layouts but also opens the possibility of guiding the conductor in more complex patterns that would not be practical otherwise. Examples include the stress-managed cos θ (82), canted cosine theta (CCT) (83), Uni-Layer (84), and Conductor on Molded Barrel (85). Potential benefits of stress-managed coil designs as well as challenges in magnetic efficiency, mechanical support, and electrical integrity are discussed in Sections 3.4 and 4.2.2.

Quench training: gradual increase of the quench current of a superconducting magnet during a sequence of repeated ramps to quench (while training may in principle remedy a lack of mechanical support, it is not viable in a large production due to cost and schedule considerations)

3.3. Mechanical Structures, Magnet Assembly, and Test Results

Superconducting accelerator magnets require strong mechanical structures to prevent conductor motion under Lorentz forces and the associated frictional energy release that may cause premature quenches and quench training. This is usually accomplished by precompressing (preloading) the coil before powering so that it remains in contact with the structure up to the design field.

Laminated collars (**Figure 6a, i**) were first developed for the Tevatron and have been adopted in most subsequent projects. A precise geometric boundary for the coil is obtained by die-stamping the laminations. The collars are locked in position with keys inserted under hydraulic presses. Coil size and elastic modulus need to be adjusted to achieve the desired preload in this fixed geometry.
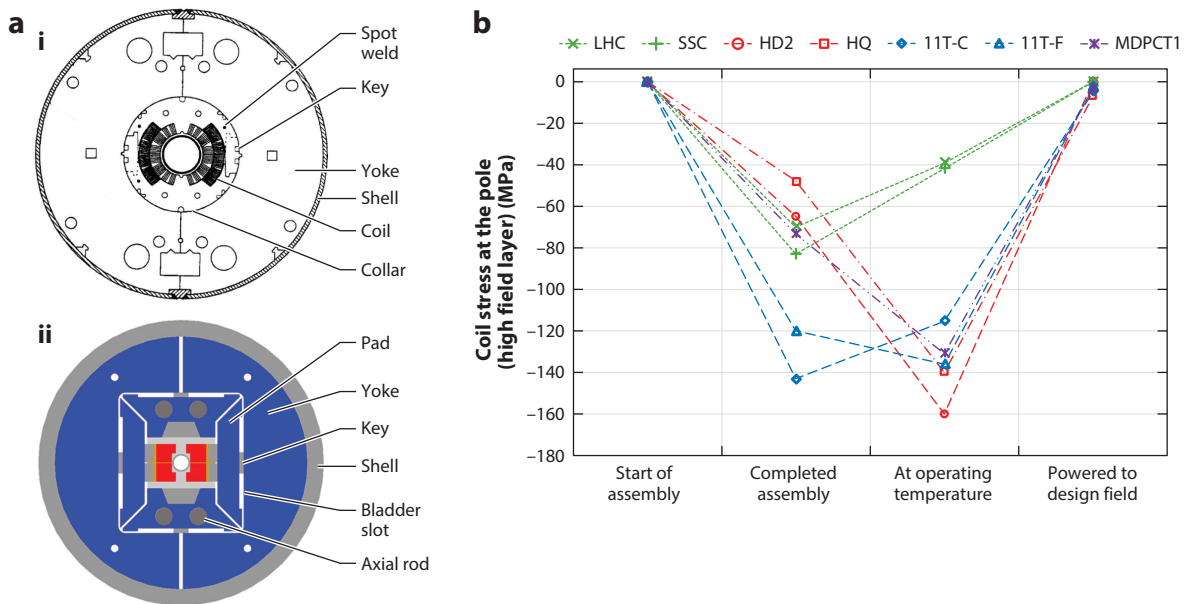

Figure 6

(a) Examples of (*i*) collar (SSC) and (*ii*) shell (HD2) structures. (*b*) Coil stress evolution during magnet fabrication, cooldown, and powering for different mechanical designs (negative values indicate compressive stress): self-supporting collar [*green*; LHC dipole (11) and SSC dipole (87)], shell [*red*; LBNL HD2 (88) and LARP HQ (94)], collar with additional support elements [*blue*; 11-T dipole: CERN design (104) and FNAL design (103)], and aluminum clamps [*purple*; FNAL MDPCT1 (89)]. Subpanel *i* of panel *a* adapted with permission from Reference 87 and Jim Strait (LBNL). Subpanel *ii* of panel *a* adapted from Reference 38 (CC BY 4.0).

Collar-based structures were successfully implemented in early Nb_3Sn dipoles in the range of 10 to 11 T (32, 33). However, impregnated coils have high elastic modulus (25–40 GPa versus 10–13 GPa in Nb-Ti LHC coils), which causes higher stress variations due to dimensional tolerances. In addition, thermal contraction differentials between collar and coil cause a loss of precompression during cooldown. As the design field increases, it becomes more difficult to apply sufficient preload without exceeding the Nb_3Sn stress degradation limits.

For these reasons, there is interest in alternative mechanical concepts to achieve a significant and predictable increase of preload at cooldown (reducing the coil stress at assembly, when degradation thresholds are lowest) and to precisely tune the assembly preload without relying on tight coil tolerances. The most developed approach (**Figure 6a**, **ii**) relies on a thick outer aluminum shell as its main structural element (86). The shell is placed in tension against the coil by splitting the iron yoke in sections and expanding the resulting gaps with water-pressurized bladders. At this stage, interference keys are inserted, and the bladders are deflated and removed. During cooldown, the shell tension further increases due to its high thermal contraction differential relative to the iron yoke. This effect can be controlled by adjusting the shell and yoke geometry or replacing aluminum with stainless steel. A conceptually similar system using aluminum or stainless-steel rods can be used to support the coil against longitudinal Lorentz forces generated at the magnet ends.

The shell structure was initially developed for the LBNL RD (36) and HD (90) dipoles. It was later adopted for the LARP Long Quadrupoles (91) following a successful scale-up demonstration in the Long Racetrack models (92) and systematic comparisons with a collar-based structure in the Technology Quadrupole models (93). An improved version including alignment features (94) was the basis for the MQXF IR Quadrupole design (95), which introduced all accelerator integration elements, including a stainless-steel pressure vessel welded over the segmented aluminum shell (42).

Shell-based structures provide a flexible mechanical support system for magnet R&D. Of particular interest is the capability to fine-tune the preload and perform a controlled disassembly. Examples include the CERN Racetrack Model Coil (96), enhanced Racetrack Model Coil (97), and Racetrack Model Magnet (98), which reached coil fields in the range of 16.2–16.7 T at 1.9 K using both RRP and PIT conductors. A shell-based structure was also adopted for the FRESCA2 dipole, built in collaboration by CERN and CEA to test cables in a high transverse field (99). After several tests with different coil and preload configurations, the magnet achieved a central field of 14.6 T in a 100-mm-round aperture (100). A Test Facility Dipole with similar characteristics and 150-mm horizontal aperture is under development at LBNL (101).

Two collar structures were developed for the HL-LHC 11-T dipole:[5] The first has a round collar with additional support from a welded skin and aluminum spacers on the iron yoke (103), and the second uses a self-supporting collar with a wedge-shaped insertion at the pole to apply azimuthal preload (104). After optimization in short models, several 5.5-m-long prototypes achieved the target field with good field quality. However, additional work is required to address instances of degradation after thermal and powering cycles.

A mechanical structure based on aluminum clamps and a stainless-steel skin was developed by FNAL for the four-layer, 60-mm-aperture MDPCT1 dipole (105). The clamps protect the coil from excessive stress during assembly and provide a well-controlled preload increase at cooldown. In its second test, the magnet achieved a maximum field of 14.5 T at 1.9 K but experienced 18% degradation after a thermal cycle (106).

---

[5]The HL-LHC 11-T dipole (102) was designed to replace four of the 8.3-T Nb-Ti arc dipoles with shorter ones made of Nb_3Sn, to provide space for additional collimators.

Accurate control of both coil geometry and preload remains a critical objective for the collider application. Continued progress in mechanical design and coil fabrication technology is required for the success of these efforts.

3.4. Performance Optimization: Stress Degradation Versus Training

Studies of magnet performance as a function of the applied preload can be used to determine the Nb_3Sn stress limits in the actual as-built environment. Interpretation of the results relies on computational models and strain gauge measurements to derive the coil stress distributions. Specific design features and fabrication processes may influence the outcome, adding to the complexity of the analysis. Nevertheless, these studies provide essential data that complement the tests performed on wires and cable samples.

Racetrack coils are well suited to study permanent degradation. The HD1 magnet achieved 95% of its conductor limit with an initial preload of 155 MPa, with some variability in the 90–95% range. This variability was removed by increasing the preload to 185 MPa, but a 2% reduction of the quench current was observed after a thermal cycle (109).

Studies performed in support of the HL-LHC program focused primarily on quadrupole configurations. The LARP TQS03 model was tested in three preload steps with average coil stresses of 120, 160, and 200 MPa (peak: 240–260 MPa). The corresponding quench levels were 93%, 91%, and 88% of the short sample limit (110). More recently, an MQXFS short model using both PIT and RRP coils was tested in the azimuthal stress range of 110 to 190 MPa in steps of 20 MPa (111). In all cases the magnet was able to operate above 90% of the short sample limit. However, signs of performance degradation (at the level of a few percent) were observed in the PIT coils above 170 MPa. In a separate test, the preload in a well-performing MQXFS short model was first reduced, causing some retraining and overall lower performance; it was then increased again, and the initial performance level was regained (112).

These results confirm that Nb_3Sn magnets can sustain the 150- to 200-MPa stress levels required for 16-T dipoles (113), but the design margins may be too narrow for a robust large-scale production. Increasing the tolerance to high stress is a conductor development priority to address this challenge (114). Alternative options are provided by stress-managed coil designs (see Section 3.2). However, the internal structures designed to protect the conductor from stress accumulation make it more difficult to apply preload, and thus there is a negative impact on the training performance (115). This has prompted a renewed interest in developing impregnation materials that are alternatives to epoxy resins to minimize the energy release due to cracking or motion (see the sidebar titled Addressing the Training Challenge in Superconducting Magnets). A dedicated test setup was developed at the University of Twente to investigate training of individual Nb_3Sn Rutherford cables in a channel, simulating the environment of grooved formers. Consistent with results from early Nb-Ti magnets, it was found that the use of paraffin wax can greatly improve performance (116). The test of a CCT dipole magnet at LBNL further confirmed this result (117), giving renewed emphasis to the search for optimized impregnation materials to address both stress and training limitations of Nb_3Sn magnets (118).

3.5. Quench Protection, Analysis, and Diagnostics

Protection of accelerator magnets has traditionally relied on quench heaters. In high-field Nb_3Sn magnets, heaters are embedded in the epoxy-impregnated coil to keep the delay from firing to quench initiation below 5–15 ms. This complicates the fabrication process and adds to the risk of insulation failures. The discharge voltage can be lowered by heating the coil only at selected locations (heating stations) and relying on quench propagation between stations (119).

Quench heaters: thin resistive strips placed along the length of the coils; upon detection of a quench, a capacitive discharge through the heaters is used to accelerate the coil transition to the normal state and dissipate the magnet's stored energy over the largest possible fraction of the coil volume

ADDRESSING THE TRAINING CHALLENGE IN SUPERCONDUCTING MAGNETS

The first observations of the training phenomenon in early Nb-Ti solenoids prompted Rutherford Lab researchers to study how different coil fillers influenced the magnet performance. Materials of low tensile strength such as oil or wax effectively eliminated training, while coils impregnated with resins still experienced premature quenches (107). It was inferred that these quenches were caused by energy release from epoxy cracking or detaching from the structure. In softer materials, internal strains are released during cooldown or at low field without building up to dangerous levels that may cause quenches.

A new paradigm emerged after the Tevatron team discovered that allowing liquid helium to permeate the cable greatly improved training performance (108). Porous insulation and high preload using collar structures became the standard approach in Nb-Ti accelerator coils. However, Nb_3Sn magnets marked a return to glass fiber insulation for compatibility with the high-temperature reaction and epoxy impregnation to protect the wires from stress concentration. These new requirements brought back the training challenge as a critical issue to be addressed in preparation for large-scale production.

Nevertheless, degradation of heater performance and coil-heater insulation is often observed after repeated firing, posing a threat to long-term reliability.

A new Coupling-Loss-Induced Quench (CLIQ) protection system was introduced at CERN in 2013 (120). An oscillating current pulse is injected directly into the magnet circuit, causing a fast change of the local magnetic field and inducing strong coupling currents that rapidly heat and quench the coil. Following a series of performance demonstrations in LARP magnets, CLIQ was integrated into the HL-LHC IR quadrupole protection system. Heaters are also being used for redundancy and to improve the overall performance (121).

The CLIQ system was made possible by a quantitative understanding of the role of interfilament coupling currents during the coil transition to the normal state (122). The improved accuracy of quench simulations benefits all protection configurations and can be coupled to mechanical analysis to study the stress generated by rapid coil thermal expansion in the cold structure (123). These capabilities bring new elements to a broad effort toward integrated modeling of high-field accelerator magnets, exemplified by the ROXIE (124) and STEAM (125) environments. Further networking of magnet design and analysis tools is underway using collaborative model-based systems engineering concepts (126).

Diagnostic capabilities are also key to detailed understanding of magnet performance. Traditional voltage taps are being complemented by acoustic measurements of mechanical disturbances (127) and new antenna designs to localize quench origins (128). Large amounts of data generated by advanced sensors and data acquisition systems are prompting the use of machine learning approaches for analysis of mechanical transient events and real-time quench detection (129).

The combined use of advanced modeling and new diagnostic capabilities provides a path to understanding the root causes of performance limitations and points toward possible solutions. A recent success involved a combination of quench localization, mechanical analysis, and new X-ray technologies to identify coil damage due to excessive strain in the MQXF coils for the HL-LHC (130).

Coupling currents: eddy currents flowing between the superconducting filaments through the copper matrix in response to a flux change

4. POTENTIAL AND CHALLENGES OF HIGH-TEMPERATURE SUPERCONDUCTORS

The discovery of high-temperature superconductivity in the copper oxides sparked research efforts in a broad range of potential applications to take advantage of their vastly superior critical

temperature and field (131). Two families of conductors are presently available for dipole development: BSSCO (in particular Bi-2212: $Bi_2Sr_2CaCu_2O_8$) and REBCO ($REBa_2Cu_3O_{7-x}$, where RE is a rare earth element, such as yttrium or gadolinium).

Bi-2212 can be formed in round multifilament wires using the PIT process in a silver matrix (132). These wires are compatible with the wind-and-react approach. However, the choices of materials for insulation, parts, and tooling are further restricted compared with Nb_3Sn because of chemical compatibility issues and higher reaction temperatures in an oxygen-rich environment (133). Strain degradation limits are also more severe (134).

REBCO is produced in multilayer tapes using deposition techniques over metal substrates, precluding a wind-and-react approach (135). Tapes are available in the range of 2 to 12 mm in width and 0.05 to 0.2 mm in thickness. The main challenge for accelerator applications is developing high-current cables that retain sufficient flexibility for coil winding. Control of magnetization effects is also an issue since the superconducting layer behaves as a single filament spanning the entire width of the tape and the tapes exhibit significant variations of J_c depending on their orientation relative to the magnetic field (**Figure 1**).

Considering that Nb_3Sn presently has performance and cost advantages at fields below $\sim$15 T, a possible design approach is combining an outer coil made of Nb_3Sn with an HTS inner coil next to the bore. This configuration is also efficient for testing different materials and concepts in relevant conditions because of the reduced size of the HTS coils and associated tooling. Recent developments in cable and coil technology for Bi-2212 and REBCO are described in the following subsections.

4.1. Bi-2212

The development of Bi-2212 Rutherford cables started at LBNL in 1998, using PIT wires produced by Showa Electric Wire and Cable Company (SWCC) for a Superconducting Magnetic Energy Storage device (136). In the following years, wires with significantly improved performance became available from both SWCC (137) and OST (138). With engineering current densities approaching the range of interest for accelerator magnets, a program to develop the relevant coil technologies was launched at LBNL (139). Rutherford cables were fabricated with 17 strands 0.8 mm in diameter (**Figure 7a,b**), and a series of small racetrack coils were wound and reacted. The initial focus was on confronting chemical compatibility issues that resulted in leakage of the core constituents through the silver matrix during reaction, causing critical
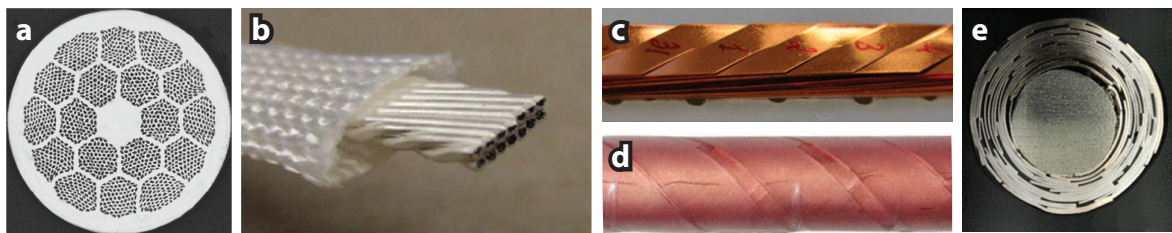

Figure 7

HTS conductors: (*a*) cross section of a 0.8-mm-diameter Bi-2212 wire, (*b*) 17-strand Bi-2212 Rutherford cable of 7.8-mm width, (*c*) YBCO Roebel cable of 12-mm width, (*d*) side view of a YBCO CORC® helical wire of 7.8-mm diameter, and (*e*) cross-sectional view of the same wire. Abbreviation: HTS, high-temperature superconductor. Panel *a* reproduced from Reference 140 with permission from AIP Publishing. Panel *b* reproduced with permission from Reference 141. Panel *c* reproduced with permission from Reference 142. Panels *d* and *e* reproduced with permission from Reference 143.

current degradation and insulation failures. The best results were obtained using INCONEL 600 for coil parts and tooling and aluminum silicate (mullite) braided sleeve insulation. Having demonstrated a more robust seal of the core in the silver-alloy tubes, OST wires became the baseline (140). Later coils did not exhibit significant leakage and achieved 2.6 kA in self-field (1 T) at 4.2 K (133). The engineering current density was 300 A mm^{-2}, and no quench training was observed.

These results suggested the need for a more fundamental understanding of Bi-2212. The Very High Field Superconducting Magnet Collaboration was formed, bringing together materials science and accelerator experts with support from the DOE Office of High Energy Physics. A key breakthrough was the discovery that large gas-filled volumes can form in the filaments during reaction (144), disrupting the current flow between Bi-2212 grains. These "bubbles" originated from the porosity of the Bi-2212 powder, which coalesced into large volumes during the melt phase.[6] To decrease the void fraction after drawing, different methods were investigated, such as cold isostatic pressing (145) and swaging (146). The most successful approach was to densify the wires during heat treatment in special furnaces providing a high-pressure (50–100 atm) flowing mix of argon and oxygen (147). This overpressure heat treatment increased the current density by a factor of three.

Another critical factor affecting the wire performance is the quality of the Bi-2212 powders, such as particle size, composition uniformity, and level of impurities. With support from the US DOE, new powder-processing capabilities were developed (16), leading to engineering current densities above 1 kA mm^{-2} up to 25 T and 4.2 K in the latest-generation wires (**Figure 1**).

These combined improvements resulted in racetrack coils achieving a quench current of 8,604 A at 4.2 K when tested individually using their reaction tooling for mechanical support. The corresponding wire J_E is 1.01 kA mm^{-2} at a 3.5-T peak field, about three to four times higher than in earlier coils of the same design (148). In another test, two coils assembled in an iron yoke and aluminum shell achieved a peak field of 4.7 T (149). This was also the first test incorporating a twisted wire, which is important for control of AC losses. However, leakage is still observed (**Figure 8a**) and is believed to be partly responsible for conductor performance degradation in the coils relative to the virgin wires (150). Additional limitations derive from variability of conductor properties and difficulties in controlling the reaction parameters, such as temperature uniformity, in the larger furnaces used for coil reaction. Work is ongoing to address these challenges while expanding the coil technology to new configurations that incorporate stress management features, such as the CCT (151) and the stress-managed cos θ (152).
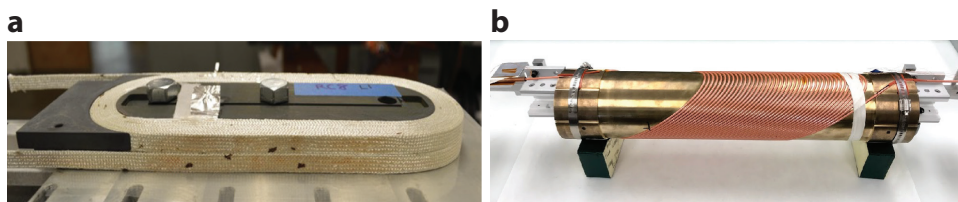
Figure 8

High-temperature superconductor coils. (*a*) Bi-2212 racetrack showing dark spots at locations where leakage was observed after reaction. (*b*) One layer of a four-layer canted cosine theta coil wound with REBCO CORC® cable. Photo in panel *a* provided by Tengming Shen, LBNL. Photo in panel *b* provided by Xiaorong Wang, LBNL.

---

[6]The powder fill factor is limited to ~70% for the wire drawing process to be successful.

4.2. REBCO

REBCO has a higher critical temperature and field than any other technical superconductor (153). After an initial period of development focused on electric utility applications, the introduction of metal substrates for mechanical reinforcement and enhanced flux pinning enabled a new generation of high-field solenoids for nuclear magnetic resonance (NMR) (154). The latest REBCO-based commercial systems are operating at 28 T (155), and research magnets have surpassed 30 T (156). However, along with these successes, significant challenges have come into focus. In particular, large screening currents flowing in high fields can produce shear forces, which cause tape delamination, and large thermal margins delay quench detection and protection, causing excessive hot spot temperatures and potential damage. In several instances, performance degradation or magnet failure was observed following a successful first ramp to a high field. Confronting these issues is expected to be even more challenging in accelerator configurations.

Two main cable concepts are being developed for application of REBCO tapes to dipole coils. In the first case, trapezoidal cuts are applied on alternating sides of a wide (>10 mm) tape (**Figure 7c**). The resulting meandering shape allows one to stack and interlock 10–15 of these tapes in a rectangular, fully transposed Roebel configuration (157). In the second case (**Figure 7d,e**), tapes are wound in a helical pattern around a core, producing a round geometry (158, 159). Various configurations are available with outer radii of 2 to 4 mm.

4.2.1. Roebel cables.
The development of dipole coils using Roebel cables has been pursued by several European programs and collaborations over the last decade (160). A critical step was addressing the transverse stress degradation, which was found to start at approximately 40 MPa in bare cables due to stress concentration at the crossing points. Impregnation of REBCO tapes can result in delamination and strong degradation due to thermal contraction differentials between epoxy and tape. However, after surrounding the Roebel cable with a fiberglass sleeve, several resins could be applied successfully, including the CTD 101K system that is extensively used in Nb_3Sn magnets (161). With this method, small samples demonstrated transverse stress limits in the range of 370 to 440 MPa. This result, if reproduced in larger coils, would fully address the needs of future high-field dipoles.

The model coil programs explored a traditional $\cos \theta$ geometry (162) and a modified block coil (named Feather) where the conductors are slightly tilted to follow the flux lines (163). This arrangement takes advantage of the higher J_c of REBCO tapes in the parallel field orientation and reduces the screening current effects by minimizing flux linkage. Different models of the Feather insert were built to optimize the fabrication methods and conductor design. The latest model, built with a high-performance conductor, achieved 4 T in a stand-alone test (164).

4.2.2. Round cables.
REBCO tapes can tolerate high compressive strain on the ceramic layer, making it possible to bend them around a small-diameter core. A flexible round conductor can then be obtained using several superimposed helical windings. Two variants are commercially available: CORC® (Conductor on Round Core) (158) and STAR® (Symmetric Tape Round) wires (159). Both types have been tested at LBNL in a CCT geometry. For the CORC, a four-layer CCT was implemented with a 65-mm aperture and 40 turns per layer (**Figure 8b**), producing a maximum field of 2.9 T at 6.3 kA and 4.2 K (165). The STAR wire uses special REBCO tapes with a reduced substrate thickness of approximately 20 μm and with the REBCO layer positioned near the neutral axis to achieve smaller bending radii around the inner core. This results in a more flexible wire that can be wound in a 50-mm aperture. The first test used a two-layer, three-turn-per-layer design with a limited conductor length of 10 m (166). Two wires were cowound in the same groove without transposition and powered in parallel. The maximum field was 0.8 T at a current of 8.9 kA.

These tests, which made it possible to gain initial experience with the use of helical wires, point toward possible improvements for both conductor and magnet design.

5. THE ROAD AHEAD: PAVING THE WAY FOR THE NEXT HADRON COLLIDER

A broad development program is required to achieve the magnet performance goals and production readiness for future hadron colliders. Comprehensive plans and timelines were formulated in support of recent strategy documents in Europe and the United States (114, 167, 168). Without attempting to capture the entire scope of these efforts, the following paragraphs provide a viewpoint on current developments that have the potential to address the most significant challenges and shape future directions.

5.1. Niobium–Tin Development

A significant increase of the Nb_3Sn critical current density at high fields may be achieved with improved pinning (29), expanding the design options to optimize magnet performance and cost-effectiveness (169). Contrary to Nb-Ti, the grain size in commercial Nb_3Sn wires (100–200 nm) is much larger than the flux line spacing at high fields (10–15 nm). Several methods have been devised to refine the grain size or introduce artificial pinning centers (170). Promising results were obtained using an NbZr precursor to generate ZrO_2 precipitates during heat treatment (171). Adding hafnium or zirconium to NbTa filaments may provide similar benefits while avoiding a degradation of the upper critical field that has been associated with the internal oxidation process (172).

Materials with high heat capacity can make the conductor more resilient to disturbances. An increase of a factor of three in the minimum quench energy was demonstrated, although the quench propagation velocity was also reduced (173). Similar to artificial pinning, the main hurdle is achieving the desired improvements without disrupting the highly optimized wire-manufacturing process. If successful, this approach could provide increased margins against flux jump instabilities and mechanical motions that cause premature quenches.

New impregnation materials may hold the answer to some critical engineering challenges facing the program. Again, the main difficulty is addressing the complete spectrum of requirements: mechanical support, electrical insulation, tolerance to thermal cycles, powering cycles, and radiation loads. Impregnation of large coils also requires low viscosity and sufficient pot life (174). From the mechanical standpoint, a balance needs to be found between providing support against motion and stress concentration, which favors hard resins, and limiting the energy release due to cracking and debonding, which favors softer materials. Each magnetic and mechanical design approach may require a different composition to achieve a fully optimized solution.

5.2. High-Temperature Superconductor Development

The special characteristics of HTS are prompting a broad exploration of technology options, requiring close guidance from magnet design studies to assess their potential benefits and the conditions for those benefits to be realized. Initial concepts combining Bi-2212, Nb_3Sn, and Nb-Ti to reach dipole fields of 20 to 24 T were introduced in connection with a possible energy upgrade of the LHC (175). Further studies of hybrid Bi-2212/Nb_3Sn layouts include an 18-T CCT (176), a 20-T common coil (177), a 20-T block coil (178), and a 20-T $\cos \theta$ coil (179). A comparison of the magnetic characteristics of these different layouts is reported in Reference 180, in which two stress-managed $\cos \theta$ options were also introduced. Preliminary design considerations relevant to 20-T dipoles using REBCO Roebel cables are reported in Reference 181, and the potential application of CORC cables in CCT dipoles is discussed in Reference 182.

From these combined efforts, a design framework for HTS dipoles is starting to take shape, and initial assessments can be made of the strengths and weaknesses of different approaches. However, additional studies are needed to cover the spectrum of conductor technologies under consideration (e.g., the design of 20-T dipoles using round REBCO cables), the feasibility of operating at 20 K in liquid hydrogen, and the conditions that would make a 24-T design possible. These studies would benefit from a set of reference scenarios with agreed-upon parameters, such as short sample field, operating temperature, and magnet aperture. From this basis, specific R&D targets may be derived for different technology options along with validation experiments to select the most promising concepts.

Testing at relevant field and stress levels is vital to progress on HTS technologies. One possible approach is assembling the HTS coils in a common structure with Nb_3Sn coils providing the background field in a range of magnetic and mechanical configurations (149). A second approach relies on permanent installations providing a high field volume where the test coil or cable can be inserted. Examples include FRESCA2 (99) and the common-coil test station at BNL (183). A 15-T facility is under development by a collaboration of Fermilab and LBNL to support HTS development for both fusion and HEP (184).

A new class of iron-based superconductors shows significant potential for high J_c at high fields with a lower cost (185). Compatibility with PIT fabrication techniques is particularly attractive. At this stage, insufficient connectivity at grain boundaries is the critical problem that limits the long-range J_c, but work is ongoing to address these issues (186). In parallel, a coil fabrication and test program is underway at IHEP in support of the SPPC magnet development (187).

5.3. Scale-Up and Industrial Production

Mass production of thousands of full-scale magnets in industry is among the most significant challenges of a future energy frontier collider. Within the dipole operating range under consideration by both FCC and SPPC, two critical transitions can be identified in terms of complexity and cost: the maximum field that can be achieved with a single, continuously wound Nb_3Sn coil module per pole (12–13 T) and the maximum field that can be achieved without introducing HTS (~16 T).

Conductor costs are expected to account for approximately 50% of the total cost of the 16-T FCC dipole system (188). The corresponding Nb_3Sn requirement is approximately 8,000 t (7), one order of magnitude larger than that of ITER,[7] which required 600 t of Nb_3Sn and achieved a peak production rate of 150 t y^{-1} using nine facilities worldwide (189). However, the wires of interest for collider magnets currently have only one supplier, and the largest production to date was of the order of 30 t for the HL-LHC. Similar factors apply to high-temperature superconductors. The HTS cross-sectional area in a twin-aperture, 20-T hybrid dipole is, at minimum, 25 cm^2 (180)— approximately 2,000 t for a 100-km machine—as opposed to the current production of the order of a few tonnes per year.

With these challenges in mind, a compact and magnetically efficient coil layout is paramount. To minimize the conductor volume, the wire and cable design can be optimized to increase the current density in the lower-field regions of the coil (grading). This can be readily accomplished in separate coil modules, while grading within a single-coil module requires a high-current connection between two subcoils, adding significant complexity. A first option is to join the cables at a location external to the winding pack (190, 191); an internal joint avoids the complexity of routing the cables outside the coil module but needs to confront limited space availability and operation in high fields (192).

---

[7]ITER is a magnetic confinement plasma physics experiment based on a large tokamak fusion reactor (**https://www.iter.org**).

An important lesson learned from the HL-LHC program is to address the requirements for high-voltage testing as early as possible in the development phase (77). This is particularly relevant to designs that incorporate internal coil structures, which greatly expand the conductor surface exposed to ground faults. Significant improvements in electrical robustness may be achieved by replacing quench heaters with a CLIQ-based protection system. Recent CLIQ implementations also eliminate the need to connect to the main circuit by using independently powered coupling coils (193).

Production of the new IR quadrupoles for the HL-LHC marks a major milestone for Nb_3Sn technology, but current methods for coil and magnet fabrication are labor-intensive and not suitable for a large number of units. Substantial industry involvement is needed to develop more robust and efficient processes and better control uniformity. In Europe, the fabrication of a two-layer, accelerator-size prototype was included in the Accelerator R&D Roadmap and is currently underway by the CERN-led HFM Collaboration (**https://hfm.web.cern.ch**) to achieve a nominal field of 12 T and an ultimate field of 13.5 T (194). In the United States, a similar proposal was formulated in the context of the Snowmass community planning effort, leveraging the experience, documentation, and lessons gained from US-built HL-LHC IR quadrupoles (195). These activities will provide a platform to develop industrialized processes, demonstrate technical performance, and formulate cost and schedule targets for large-scale production.

5.4. Synergies and Collaborations

The history of superconductivity is one of collaboration among science and engineering disciplines and of synergies in applications ranging from NMR/magnetic resonance imaging (MRI) to accelerators, fusion, and electric power (108). For example, the Tevatron project, made possible by multifilament wires developed for small research solenoids, promoted performance improvements and production capabilities that launched the NMR/MRI industry and, in turn, enabled larger accelerator projects. Early Nb_3Sn dipoles used bronze-route wires developed for research and fusion. Later on, high-performance wires developed by HEP researchers were applied to the ITER production (189). Next-generation fusion devices are currently driving a production scale-up of HTS tapes, which may benefit a broad range of applications.

Within the particle physics program, there are significant overlaps in the magnet technology needs of future hadron and muon colliders (196), including dipoles for the collider ring, fast ramping magnets for the injectors, and HTS-based solenoids for muon cooling. High-field dipoles and solenoids are also of interest for next-generation axion dark matter experiments (167). Recent community planning efforts have provided opportunities for coordination of magnet development plans in Europe (114), the United States (197), China (198), and Japan (199). University groups continue to be the incubators of new ideas while training future scientists and engineers. Industry involvement is required for conductor procurement and the development of robust fabrication processes. These strong synergies across HEP and with the broader community will continue to foster a stimulating research environment and benefit all applications.

SUMMARY POINTS

1. High-field superconducting magnets are the enabling technology for past and future hadron colliders, at the intersection of materials science, accelerator physics, and large-scale engineering.

2. Niobium–tin (Nb_3Sn) is entering the accelerator arena with a high-profile interaction region quadrupole upgrade that will enable a 10-fold increase of the integrated luminosity of the LHC. This technology has a clear path to meet all requirements for the next hadron collider with further technical optimization and more robust processes for large-scale production.

3. Advanced modeling and diagnostics are marking a transition from empirical explorations to precise analysis of the performance boundaries of brittle superconductors.

4. Initial steps are being taken toward future high-temperature superconductor (HTS) dipoles that could open the way to a new generation of high-performance and sustainable accelerators.

FUTURE ISSUES

1. A fundamental and far-reaching question is whether the extraordinary properties of HTS can be harnessed in practical accelerator dipoles. This will require a combination of convincing experimental demonstrations and design studies that address the complex requirements of energy frontier colliders. At present, performance and cost considerations strongly favor an approach based on hybrid LTS-HTS coils. In the longer term, HTS production scale-up and cost reduction may open the way to all-HTS magnets operating at higher temperatures.

2. For both LTS and HTS, testing in relevant configurations at high fields is required to demonstrate the applicability of promising new approaches to cable design, coil fabrication, and mechanical structures. Efficient test infrastructure will enable faster progress toward the optimal solutions.

3. Materials science breakthroughs may still provide the best opportunities to advance conductor and magnet technologies for future hadron colliders. Examples include Nb_3Sn and Bi-2212 wires with higher critical current density and stress tolerance, high-current REBCO cables with lower magnetization and sufficient flexibility for coil winding, cost-effective iron-based superconductors produced in round wires, and new impregnation materials with properties optimized for specific magnet designs.

4. Significant synergies exist between the magnet needs of future hadron colliders, muon colliders, and the broader applications of high-field conductors to nuclear magnetic resonance and fusion devices. Strong connections among these programs will result in faster progress and help sustain the long-term R&D effort.

DISCLOSURE STATEMENT

The author is not aware of any affiliations, memberships, funding, or financial holdings that might be perceived as affecting the objectivity of this review.

ACKNOWLEDGMENTS

LITERATURE CITED

1. Edwards H. *Annu. Rev. Nucl. Part. Sci.* 35:605 (1985)
2. Tollestrup A, Todesco E. In *Reviews of Accelerator Science and Technology*, ed. A Chao, W Chou, Vol. 11, pp. 185–210. Singapore: World Sci. (2008)
3. Rossi L. *IEEE Trans. Appl. Supercond.* 12:219 (2002)
4. Schoerling D, Zlobin AV, eds. *Nb₃Sn Accelerator Magnets: Designs, Technologies and Performance*. Cham, Switz.: Springer (2019)
5. Brüning O, Klein M, Rossi L, Spagnolo P, eds. *The Future of the Large Hadron Collider*. Singapore: World Sci. (2023)
6. Schoerling D, et al. *IEEE Trans. Appl. Supercond.* 29(5):4003109 (2019)
7. Abada A, et al. (FCC Collab.) *Eur. Phys. J. Spec. Top.* 228:755 (2019)
8. Tang J. *Front. Phys.* 10:828878 (2022)
9. Abada A, et al. (FCC Collab.) *Eur. Phys. J. Spec. Top.* 228:1109 (2019)
10. Benedikt M, Zimmermann F. *FCC feasibility study status*. Presented at FCC Week 2023, London, June 5–9 (2023)
11. Bruning O, et al. Report 2004-003, CERN, Geneva (2004)
12. Todesco E, Zimmermann F, eds. Yellow Report 2011-3, CERN, Geneva (2011)
13. Boutboul T, et al. *IEEE Trans. Appl. Supercond.* 16(2):1184 (2006)
14. Kanithi H, et al. *IEEE Trans. Appl. Supercond.* 24:6000504 (2014)
15. Parrell JA, et al. *IEEE Trans. Appl. Supercond.* 13(2):3470 (2003)
16. Jiang J, et al. *IEEE Trans. Appl. Supercond.* 29(5):6400405 (2019)
17. Braccini V, et al. *Supercond. Sci. Technol.* 24:035001 (2011)
18. Ballarino A, et al. *IEEE Trans. Appl. Supercond.* 29(5):6001709 (2019)
19. Sorbi M, et al. *IEEE Trans. Appl. Supercond.* 27(4):4001205 (2017)
20. Bellafont I, et al. *Phys. Rev. Accel. Beams* 23:033201 (2020)
21. Xu Q, et al. *IEEE Trans. Appl. Supercond.* 25(3):4000905 (2015)
22. Buffat X, Schulte D. In *Proceedings of IPAC'16*, pp. 1426–29. Geneva: CERN (2016)
23. Giovannozzi M. *EPJ Tech. Instrum.* 9:5 (2022)
24. Wolf R. Report LHC-M-ES-0001, CERN, Geneva (2001)
25. Dalena B, et al. In *Proceedings of IPAC'18*, pp. 137–40. Geneva: JACoW (2018)
26. Izquierdo Bermudez S, et al. *IEEE Trans. Appl. Supercond.* 29(5):4901705 (2019)
27. Matthias BT, et al. *Phys. Rev.* 95(6):1435 (1954)
28. Kunzler JE, Buehler E, Hsu FSL, Wernick JH. *Phys. Rev. Lett.* 6:89 (1961)
29. Godeke A. *Supercond. Sci. Technol.* 19:R68 (2006)
30. Hashimoto Y, Yoshizaki K, Tanaka M. In *Proceedings of the 5th International Cryogenic Engineering Conference*, ed. K Mendelssohn, pp. 332–35. Guildford, UK/Kyoto, Jpn.: IPC Sci. Technol. Press/Cryog. Assoc. Jpn. (1974)
31. Rossi L, Zlobin AV. See Ref. 4, pp. 53–84 (2019)
32. Asner A, Perin R, Wenger S, Zerobin F. In *11th International Conference on Magnet Technology (MT-11)*, ed. T Sekiguchi, S Shimamoto, pp 36–41. Dordrecht, Neth.: Springer (1990)
33. den Ouden A, Wessel S, Krooshoop E, ten Kate H. *IEEE Trans. Appl. Supercond.* 7(2):733 (1997)
34. McInturff A, et al. In *Proceedings of the 1997 Particle Accelerator Conference*, Vol. 3, pp. 3212–14. Piscataway, NJ: IEEE (1997)

35. Field M, et al. *IEEE Trans. Appl. Supercond.* 11(1):3692 (2001)
36. Caspi S, et al. *IEEE Trans. Appl. Supercond.* 11(1):2272 (2001)
37. Gourlay SA. See Ref. 4, pp. 343–70 (2019)
38. Sabbi G. See Ref. 4, pp. 285–310 (2019)
39. Gourlay SA, et al. *IEEE Trans. Appl. Supercond.* 16(2):324 (2006)
40. Sabbi G. *IEEE Trans. Appl. Supercond.* 23(3):4000707 (2013)
41. Ambrosio G, et al. *IEEE Trans. Appl. Supercond.* 33(5):4003508 (2023)
42. Izquierdo Bermudez S, et al. *IEEE Trans. Appl. Supercond.* 33(5):4001209 (2023)
43. Bottura L, Prestemon S, Rossi L, Zlobin AV. *Front. Phys.* 10:935196 (2022)
44. Gallagher-Daggitt GE. Report RHEL-M-A25, Rutherford High Energy Lab., Chilton, UK (1973)
45. Scanlan RM, Dietderich DR. *IEEE Trans. Appl. Supercond.* 13(2):1536 (2003)
46. Boutboul T, et al. *J. Phys. Conf. Ser.* 97:012211 (2008)
47. Lindenhovius JH, et al. *IEEE Trans. Appl. Supercond.* 9(2):1451 (1999)
48. Ferracin P, et al. *IEEE Trans. Appl. Supercond.* 26(4):4000207 (2016)
49. Tarantini C, et al. *Supercond. Sci. Technol.* 27:065013 (2014)
50. Field MB, et al. *IEEE Trans. Appl. Supercond.* 24(3):6001105 (2014)
51. Todesco E, et al. *Supercond. Sci. Technol.* 34:053001 (2021)
52. Ferracin P, et al. *IEEE Trans. Appl. Supercond.* 29(5):4001309 (2019)
53. Swartz PS, Bean CP. *J. Appl. Phys.* 39(11):4991 (1968)
54. Ghosh AK, et al. *Supercond. Sci. Technol.* 18:L5 (2005)
55. Bordini B, Rossi L. *IEEE Trans. Appl. Supercond.* 19(3):2470 (2009)
56. Ambrosio G, et al. *IEEE Trans. Appl. Supercond.* 22(3):4003804 (2012)
57. Cheggour N, et al. *Sci. Rep.* 9:5466 (2019)
58. Ferradas Troitino J, et al. *Supercond. Sci. Technol.* 34:035008 (2021)
59. Ekin JW. *Cryogenics* 20:611 (1980)
60. ten Haken B, Godeke A, ten Kate HHJ. *J. Appl. Phys.* 85(6):3247 (1999)
61. Cheggour N, et al. *Supercond. Sci. Technol.* 23:052002 (2010)
62. Vallone G, et al. *Supercond. Sci. Technol.* 34:025002 (2021)
63. Duvauchelle J-E, Bordini B, Fleiter J, Ballarino A. *IEEE Trans. Appl. Supercond.* 28(4):4802305 (2018)
64. Puthran K, et al. *IEEE Trans. Appl. Supercond.* 33(5):8400406 (2023)
65. Flükiger R, et al. *IEEE Trans. Appl. Supercond.* 23(3):8001404 (2013)
66. Barzi E, Zlobin AV. *IEEE Trans. Nucl. Sci.* 63(2):783 (2016)
67. Dietderich DR. *IEEE Trans. Appl. Supercond.* 17(2):1481 (2007)
68. Borgnolutti F, et al. *IEEE Trans. Appl. Supercond.* 24(3):4003005 (2014)
69. Wang X, et al. *IEEE Trans. Appl. Supercond.* 24(3):4002607 (2014)
70. Collings EW, et al. *IEEE Trans. Appl. Supercond.* 27(4):0601305 (2017)
71. Borgnolutti F, et al. *IEEE Trans. Appl. Supercond.* 25(3):4002505 (2015)
72. Rossi L, Todesco E. *Phys. Rev. Spec. Top. Accel. Beams* 10:112401 (2007)
73. Caspi S, et al. *IEEE Trans. Appl. Supercond.* 19(3):1221 (2009)
74. Felice H, et al. *IEEE Trans. Appl. Supercond.* 22(3):4001904 (2012)
75. Ambrosio G, et al. *IEEE Trans. Appl. Supercond.* 19(3):1231 (2009)
76. Todesco E, et al. *IEEE Trans. Appl. Supercond.* 24(3):4003305 (2014)
77. Ambrosio G, et al. *IEEE Trans. Appl. Supercond.* 31(5):4001105 (2021)
78. Gupta R. In *Proceedings of the 1997 Particle Accelerator Conference*, Vol. 3, pp. 3344–46. Piscataway, NJ: IEEE (1997)
79. Sabbi G, et al. *IEEE Trans. Appl. Supercond.* 10(1):330 (2000)
80. Sabbi G, et al. *IEEE Trans. Appl. Supercond.* 11(1):2280 (2001)
81. McInturff A, et al. *IEEE Trans. Appl. Supercond.* 17(2):1157 (2007)
82. Zlobin AV, Kashikhin VV, Novitski I. In *Proceedings of IPAC'18*, pp. 2738–41. Geneva: JACoW (2018)
83. Caspi S, et al. *IEEE Trans. Appl. Supercond.* 24(3):4001804 (2014)
84. Rudeiros Fernández JL, Ferracin P. *Supercond. Sci. Technol.* 36:055003 (2023)
85. Kashikhin VV, Lombardo V, Velev G. In *Proceedings of IPAC'19*, pp. 4307–10. Geneva: JACoW (2019)

86. Hafalia RR, et al. *IEEE Trans. Appl. Supercond.* 12(1):47 (2002)
87. Strait J, et al. In *Conference Record of the 1991 IEEE Particle Accelerator Conference*, Vol. 4, pp. 2176–78. New York: IEEE (1991)
88. Ferracin P, et al. *IEEE Trans. Appl. Supercond.* 16(2):378 (2006)
89. Novitski I, et al. *IEEE Trans. Appl. Supercond.* 26(4):4001007 (2016)
90. Hafalia AR, et al. *IEEE Trans. Appl. Supercond.* 14(2):283 (2004)
91. Ambrosio G, et al. *IEEE Trans. Appl. Supercond.* 21(3):1858 (2011)
92. Wanderer P, et al. *IEEE Trans. Appl. Supercond.* 18(2):171 (2008)
93. Bossert RC, et al. *IEEE Trans. Appl. Supercond.* 19(3):1226 (2009)
94. Caspi S, et al. *IEEE Trans. Appl. Supercond.* 20(3):144 (2010)
95. Ambrosio G, Ferracin P. See Ref. 5, pp. 121–33 (2023)
96. Perez JC, et al. *IEEE Trans. Appl. Supercond.* 26(4):4004906 (2016)
97. Perez JC, et al. *IEEE Trans. Appl. Supercond.* 32(6):4005105 (2022)
98. Gautheron E, et al. *IEEE Trans. Appl. Supercond.* 33(5):4004108 (2023)
99. Rochepault E, Ferracin P. See Ref. 4, pp. 311–40 (2019)
100. Willering G, et al. *IEEE Trans. Appl. Supercond.* 29(5):4004906 (2019)
101. Vallone G, et al. *IEEE Trans. Appl. Supercond.* 31(5):9500406 (2021)
102. Bottura L, de Rijk G, Rossi L, Todesco E. *IEEE Trans. Appl. Supercond.* 22(3):4002008 (2012)
103. Zlobin AV. See Ref. 4, pp. 193–222 (2019)
104. Bordini B, et al. See Ref. 4, pp. 223–58 (2019)
105. Novitski I, Zlobin AV. In *Proceedings of NAPAC2016*, pp. 137–39. Geneva: JACoW (2016)
106. Zlobin AV, et al. *IEEE Trans. Appl. Supercond.* 31(5):4000506 (2021)
107. Smith PF, Colyer B. *Cryogenics* 15(4):201 (1975)
108. Wilson MN. *IEEE Trans. Appl. Supercond.* 22(3):3800212 (2012)
109. Lietzke A, et al. *IEEE Trans. Appl. Supercond.* 15(2):1123 (2005)
110. Felice H, et al. *IEEE Trans. Appl. Supercond.* 21(3):1849 (2011)
111. Mangiarotti F, et al. *Performance of a HL-LHC Nb₃Sn quadrupole magnet in the 100-200 MPa range of azimuthal stress*. Paper presented at the Applied Superconductivity Conference (ASC 2024), Salt Lake City, UT, Sept. 1–6 (2024)
112. Izquierdo Bermudez S, et al. *IEEE Trans. Appl. Supercond.* 32(6):4007106 (2022)
113. Valente R, et al. *IEEE Trans. Appl. Supercond.* 29(5):4003005 (2019)
114. Védrine P, et al. In *European Strategy for Particle Physics: Accelerator R&D Roadmap*, ed. N Mounet, pp. 9–59. Geneva: CERN (2022)
115. Arbelaez D, et al. *IEEE Trans. Appl. Supercond.* 32(6):4003207 (2022)
116. Otten S, et al. *IEEE Trans. Appl. Supercond.* 33(5):4003605 (2023)
117. Arbelaez D, et al. *Supercond. Sci. Technol.* 37:065015 (2024)
118. Barzi E, et al. *Supercond. Sci. Technol.* 37:045008 (2024)
119. Felice H, et al. *IEEE Trans. Appl. Supercond.* 19(3):2458 (2009)
120. Ravaioli E, et al. *IEEE Trans. Appl. Supercond.* 24(3):0500905 (2014)
121. Ravaioli E, et al. *IEEE Trans. Appl. Supercond.* 27(4):4702107 (2017)
122. Ravaioli E, et al. *IEEE Trans. Appl. Supercond.* 27(4):4000508 (2017)
123. Vallone G, et al. *IEEE Trans. Appl. Supercond.* 34(5):4704006 (2024)
124. Russenschuck S. *Field Computation for Accelerator Magnets: Analytical and Numerical Methods for Electromagnetic Design and Optimization*. Weinheim, Ger.: Wiley-VCH (2010)
125. Bortot L, et al. *IEEE Trans. Appl. Supercond.* 28(3):4900706 (2018)
126. Maciejewski M, et al. *IEEE Trans. Appl. Supercond.* 33(5):4003105 (2023)
127. Marchevsky M, et al. *Cryogenics* 69:50 (2015)
128. Marchevsky M, et al. *IEEE Trans. Appl. Supercond.* 27(4):9000505 (2017)
129. Hoang D, et al. *IEEE Trans. Appl. Supercond.* 31(5):4900805 (2021)
130. Moros A, et al. *IEEE Trans. Appl. Supercond.* 33(5):4000208 (2023)
131. Uglietti D. *Supercond. Sci. Technol.* 32:053001 (2019)
132. Larbalestier D, et al. *Nat. Mater.* 13:375 (2014)

133. Godeke A, et al. *Supercond. Sci. Technol.* 23:034022 (2010)
134. Dietderich DR, et al. *Phys. C Supercond.* 341–348(Part 4):2599 (2000)
135. Jin S, et al. *Appl. Phys. Lett.* 51:943 (1987)
136. Hasegawa T, et al. *IEEE Trans. Appl. Supercond.* 11(1):3034 (2001)
137. Hasegawa T, et al. *IEEE Trans. Appl. Supercond.* 12(1):1136 (2002)
138. Marken KR, et al. *IEEE Trans. Appl. Supercond.* 13(2):3335 (2003)
139. Godeke A, et al. *IEEE Trans. Appl. Supercond.* 17(2):1149 (2007)
140. Miao H, et al. *AIP Conf. Proc.* 986(1):423 (2008)
141. Godeke A, et al. *IEEE Trans. Appl. Supercond.* 18(2):516 (2008)
142. Grilli F, Vojenčiak M, Kario A, Zermeño V. *IEEE Trans. Appl. Supercond.* 26(4):4803005 (2016)
143. Mulder T, et al. *IEEE Trans. Appl. Supercond.* 26(4):4803705 (2016)
144. Kametani F, et al. *Supercond. Sci. Technol.* 24:075009 (2011)
145. Jiang J, et al. *Supercond. Sci. Technol.* 24(8):082001 (2011)
146. Jiang J, et al. *IEEE Trans. Appl. Supercond.* 23(3):6400206 (2013)
147. Matras MR, et al. *Supercond. Sci. Technol.* 29:105005 (2016)
148. Shen T, et al. *Sci. Rep.* 9:10170 (2019)
149. Shen T, Garcia Fajardo L. *Instruments* 4:17 (2020)
150. Zhang K, et al. *Supercond. Sci. Technol.* 31:105009 (2018)
151. Shen T, et al. *Phys. Rev. Accel. Beams* 25:122401 (2022)
152. Zlobin AV, Novitski I, Barzi E. *Instruments* 4:29 (2020)
153. Senatore C, et al. *Supercond. Sci. Technol.* 29:014002 (2016)
154. Selvamanickam V, et al. *Supercond. Sci. Technol.* 28:104003 (2015)
155. Wikus P, et al. *Supercond. Sci. Technol.* 35:033001 (2022)
156. Bai H, et al. *IEEE Trans. Appl. Supercond.* 30(4):4300405 (2020)
157. Goldacker W, et al. *Supercond. Sci. Technol.* 27:093001 (2014)
158. Weiss JD, et al. *Supercond. Sci. Technol.* 33:044001 (2020)
159. Kar S, et al. *Supercond. Sci. Technol.* 33:094001 (2020)
160. Rossi L, Senatore C. *Instruments* 5(1):8 (2021)
161. Gao P, et al. *Supercond. Sci. Technol.* 32:055006 (2019)
162. Durante M, et al. *IEEE Trans. Appl. Supercond.* 30(4):4602505 (2020)
163. Kirby GA, et al. *IEEE Trans. Appl. Supercond.* 27(4):4003307 (2017)
164. Araujo DM, et al. *IEEE Trans. Appl. Supercond.* 30(4):4003605 (2020)
165. Wang X, et al. *Supercond. Sci. Technol.* 34:015012 (2021)
166. Wang X, et al. *Supercond. Sci. Technol.* 35:125011 (2022)
167. Butler JN, Chivukula RS, Peskin ME, eds. Report FERMILAB-CONF-23-008/SLAC-PUB-17717, Fermi Natl. Accel. Lab./SLAC Natl. Accel. Lab., Batavia, IL/Menlo Park, CA (2023)
168. Izquierdo Bermudez S, Sabbi G, Zlobin AV. arXiv:2208.13349 [physics.acc-ph] (2022)
169. Sabbi G, et al. *IEEE Trans. Appl. Supercond.* 25(3):4001407 (2015)
170. Xu X. *Supercond. Sci. Technol.* 30(9):093001 (2017)
171. Xu X, Peng X, Sumption M, Collings EW. *IEEE Trans. Appl. Supercond.* 27(4):6000105 (2017)
172. Balachandran S, et al. *Supercond. Sci. Technol.* 32:044006 (2019)
173. Xu X, Zlobin AV, Peng X, Li P. *IEEE Trans. Appl. Supercond.* 29(5):6000404 (2019)
174. Yin S, Arbelaez D, Swanson J, Shen T. *IEEE Trans. Appl. Supercond.* 29(5):7800205 (2019)
175. Todesco E, Bottura L, De Rijk G, Rossi L. *IEEE Trans. Appl. Supercond.* 24(3):4004306 (2014)
176. Caspi S, et al. *IEEE Trans. Appl. Supercond.* 25(3):4000205 (2015)
177. Xu Q, et al. *IEEE Trans. Appl. Supercond.* 26(4):4000404 (2016)
178. Rochepault E, Ferracin P, Vallone G. *IEEE Trans. Appl. Supercond.* 32(6):4003505 (2022)
179. Marinozzi V, Ferracin P, Vallone G. *IEEE Trans. Appl. Supercond.* 33(5):4003805 (2023)
180. Ferracin P, et al. *IEEE Trans. Appl. Supercond.* 32(6):4000906 (2022)
181. van Nugteren J, et al. *IEEE Trans. Appl. Supercond.* 28(4):4008509 (2018)
182. Wang X, et al. *IEEE Trans. Appl. Supercond.* 33(5):4000608 (2023)
183. Gupta R, et al. *IEEE Trans. Appl. Supercond.* 28(3):4002305 (2018)

184. Velev GV, et al. *IEEE Trans. Appl. Supercond.* 31(5):9500304 (2021)
185. Hosono H, Yamamoto A, Hiramatsu H, Ma Y. *Mater. Today* 21(3):278 (2018)
186. Kametani F, et al. arXiv:2203.07551 [cond-mat.supr-con] (2022)
187. Zhang Z, et al. *Supercond. Sci. Technol.* 34:035021 (2021)
188. Schoerling D, et al. *IEEE Trans. Appl. Supercond.* 27(4):4003105 (2017)
189. Devred A, et al. *Supercond. Sci. Technol.* 27:044001 (2014)
190. Rochepault E, et al. *IEEE Trans. Appl. Supercond.* 30(4):4001005 (2020)
191. Calvelli V, et al. *IEEE Trans. Appl. Supercond.* 31(5):4002706 (2021)
192. Kumar M, D'Auria V, Uglietti D, Bruzzone P. *IEEE Trans. Appl. Supercond.* 29(5):4800805 (2019)
193. Mulder T, et al. *IEEE Trans. Appl. Supercond.* 33(5):4702105 (2023)
194. Levi F, et al. *IEEE Trans. Appl. Supercond.* 33(5):4000805 (2023)
195. Ambrosio G, et al. arXiv:2203.07654 [physics.acc-ph] (2022)
196. Casarsa M, Lucchesi D, Sestini L. *Annu. Rev. Nucl. Part. Sci.* 74:233 (2024)
197. Ambrosio G, et al. arXiv:2203.13985 [physics.acc-ph] (2022)
198. Xu Q. *Progress of the high field magnet program for the next-generation accelerators*. Presented at the High Field Magnet Collaboration Annual Meeting 2023, Geneva, Oct. 30–Nov. 2 (2023)
199. Ogitsu T, et al. arXiv:2203.12118 [physics.acc-ph] (2022)